



THE UNIVERSITY *of* EDINBURGH

Edinburgh Research Explorer

## Multistatic radar-based imaging in layered and dispersive media for biomedical applications

### Citation for published version:

Ullah, R, Saied, I & Arslan, T 2023, 'Multistatic radar-based imaging in layered and dispersive media for biomedical applications', *Biomedical Signal Processing and Control*, vol. 82, 104568. <https://doi.org/10.1016/j.bspc.2023.104568>

### Digital Object Identifier (DOI):

[10.1016/j.bspc.2023.104568](https://doi.org/10.1016/j.bspc.2023.104568)

### Link:

[Link to publication record in Edinburgh Research Explorer](#)

### Document Version:

Peer reviewed version

### Published In:

Biomedical Signal Processing and Control

### General rights

Copyright for the publications made accessible via the Edinburgh Research Explorer is retained by the author(s) and / or other copyright owners and it is a condition of accessing these publications that users recognise and abide by the legal requirements associated with these rights.

### Take down policy

The University of Edinburgh has made every reasonable effort to ensure that Edinburgh Research Explorer content complies with UK legislation. If you believe that the public display of this file breaches copyright please contact [openaccess@ed.ac.uk](mailto:openaccess@ed.ac.uk) providing details, and we will remove access to the work immediately and investigate your claim.



# Multistatic Radar-based Imaging in Layered and Dispersive Media for Biomedical Applications

Rahmat Ullah<sup>a,\*</sup>, Imran Saied<sup>a</sup>, Tughrul Arslan<sup>a</sup>

*<sup>a</sup>School of Engineering, The University of Edinburgh,  
Edinburgh, EH9 3JW, Scotland, United Kingdom*

---

## Abstract

This paper presents a novel algorithm for near-field radar imaging in layered and dispersive media with application to biomedical imaging. The proposed algorithm compensates for variations in the dielectric properties and integrates each component's frequency response to form an image. The algorithm uses both the amplitude and phase of the complex electromagnetic field. The proposed algorithm resolves dispersion issues using frequency-dependent velocity. The algorithm uses phase shift instead of time delay to overcome the disadvantage of time-shift radar-based methods, such as inaccurate signal transformation and wave flight time. Therefore, the proposed algorithm allows detecting small changes in dispersive media such as the human brain. The algorithm is validated using experimental data for different volumes of brain tissue affected by the accumulation of plaques and tangles due to Alzheimer's disease. The accuracy and robustness of the proposed algorithm are evaluated using estimation factor and localisation error. A maximum estimation factor of 1.1 cm and localisation error of 5.3 mm in the actual and detected volume ensure that the proposed algorithm detects small changes in the brain more accurately. The paper also discusses comparisons with radar-based algorithms, demonstrating that the proposed algorithm is less compute-intensive and yields more accurate results.

*Keywords:* Microwave Imaging, Alzheimer's Disease, Image reconstruction, radar-based algorithm, Frequency-domain measurements

---

\*Corresponding Author

*Email address:* Email: rahmat.orakzai@ed.ac.uk (Rahmat Ullah)

## 1. Introduction

Microwave imaging and sensing techniques have been investigated for detecting various biological diseases such as breast cancer, brain stroke, and, neurodegenerative diseases due to their low cost and ease of use [1]. Alzheimer's disease (AD) induces pathological changes in the human brain, including the accumulation of beta-amyloid plaques and neurofibrillary tangles caused by tau proteins. Various techniques, such as positron emission tomography (PET), have been used to monitor and image these changes in the brain [2]. However, PET scans rely on injecting biomarkers to highlight brain areas affected by these anomalies, rendering them invasive and difficult for patients to use. As a result, there is a need for imaging modalities that can noninvasively monitor AD in the human brain.

AD can be detected at the early stages by observing pathological changes such as extracellular plaques and intracellular neurofibrillary pathology in the brain even before the onset of symptoms [3]. There is a close relationship between AD development and the concentration of beta-amyloid and phosphorylated tau proteins [4]. Microwave medical imaging and sensing techniques are promising technology being investigated for breast cancer and stroke detection. It detects anomalies based on changes in the dielectric constants of the tissues. Although the technology is still in its infancy, its application for noninvasively detecting AD has recently been discovered [1]. A recent study reported that healthy and AD-affected post-mortem brain tissue samples exhibit distinct dielectric properties at different microwave frequencies [5]. According to the study, there is an increase of 82.5% and 115% in the conductivity of grey matter at 0.77 GHz and 2.4 GHz, respectively. Similarly, at 0.77 GHz and 2.4 GHz, white matter's conductivity increased by 26.2% and 63.03%, respectively, compared to healthy brain samples. This is due to the higher level of proteins in the AD-affected brain samples.

Most of the radar-based microwave imaging algorithms, such as delay-and-sum (DAS), delay-multiply-and-sum (DMAS), confocal microwave imaging (CMI), and microwave imaging via space-time (MIST) rely on the time shift (TS) of an ultra-wideband (UWB) signal between an antenna and an imaging point [6] [7]. Most of these algorithms are based on time delay, where the scattered signals in the time domain are thoroughly delayed and summed to reconstruct images of high contrast. This requires correctly evaluating the TS of a signal between an antenna and a focal point. However, in many applications, especially medical imaging, objects under test are covered by dispersive layers. The different frequency components of the UWB signal propagate with different velocities and may travel in different paths from one medium to another. In these scenarios, TS cannot be accurately estimated, leading to inaccurate results. Moreover, high-frequency components of UWB

signals attenuate more than lower-frequency components, causing bandwidth reduction that ultimately degrades imaging resolution [8]. Therefore, algorithms that rely on TS, assuming all UWB signal components travel at the same velocity, do not allow for accurate detection and localisation of objects/anomalies, especially in dispersive media. On the other hand, classical synthetic aperture radar-based algorithms entail a single transmitter element that rotates/moves around the object to mimic a larger aperture for better resolution. This imaging algorithm uses the signals phase shift (PS) instead of its magnitude values. The attenuation of the magnitude of the reflected signal depends on many factors, such as radar cross-section, distance from the antennas to the imaged object and attenuation of EM waves in the respective medium [9].

The time-domain radar-based algorithms rely on the estimation of correct sample rate time delay calculation and require transformation algorithms such as Fourier transforms if the original signal is obtained in the frequency domain [10]. In the time domain measurement, the signals are often distorted while propagating through a lossy media, which degrades the quality and accuracy of reconstructed images. Conversely, frequency-based algorithms have several advantages: avoiding transformations and tackling frequency-dependent effects such as dispersion and attenuation [11]. A frequency-based technique based on frequency signals for brain stroke detection utilising the Mathieu function was presented in [12]. The imaging region was segmented into pixels, and the energy of each pixel was calculated by solving the scattering equation using the Mathieu function. The technique mitigates multiple reflections by considering frequency-dependent wave propagation affection into account. However, it requires data from a dense antenna array with a high sampling frequency, making it computationally expensive. A similar multistatic imaging algorithm was proposed for brain injury detection in [13]. The technique used the Bessel function to calculate the scattered power inside the imaged tissue. The technique is susceptible to false targets and needs sophisticated clutter removal techniques.

An algorithm based on PS instead of TS was proposed and validated by localising objects exposed in the air [14]. The proposed algorithm is based on the confocal DAS. The algorithm used the PS values instead of the time-shift values commonly used in radar-based microwave imaging algorithms. The algorithm discards the magnitude and does not consider signal attenuation. The algorithm is further modified to localise objects in dispersive media [11]. The proposed algorithm inherited the advantages of radar-based algorithms and eliminated some of its drawbacks, such as accurate distance estimation and adding weight to signals. However, the algorithm is highly susceptible to inconsistencies during measurements of phase differences. These algorithms are evaluated by detecting solid wood and metal objects. However it is mentioned that it could potentially be used for biomedical applications. These algorithms will need to compensate for the dispersive nature of human tissue before being used for medical imaging.

Furthermore, the downside of these approaches is scattering null values where the magnitude of the incident and reflected wave becomes equal, leading to an unspecified phase.

There are various frequency-based techniques used for boundary detection of imaged tissue, to improve the accuracy. For example, a method based on the antenna's resonant frequency and the locations of the antenna was presented in [15]. The method estimated the boundary of an imaged object based on shifts in the resonant frequency of the antenna while facing the imaged object. The method provides sensible accuracy; however, it requires a virtual antenna array to increase the number of boundary points surrounding the object. This technique is also limited to a range of distances, having a constant trend [16]. The proposed algorithm is based on microwave scattering parameters that use both PS and amplitude to form an image. The main principle is to detect the amplitude and phase variations of the reflection coefficient propagating through areas of interest such as skin, skull, cerebrospinal fluid (CSF), grey matter, and white matter. The phase and amplitude are compensated for each frequency component in the scattering signals. The compensated signals are integrated over the spectrum (low-end to high-end frequency) to characterize the individual layers of different tissue in the brain. Since the algorithm relies on PS to detect the region of interest, it overcomes the drawbacks of the traditional radar-based imaging algorithm. It enables the detection of small changes/anomalies in the dispersive and layered media more accurately. The novel aspects of the proposed algorithm are:

- Avoid transformation issues such as correct estimation of the time step, required in time domain DAS-based algorithms, where signal obtained in the frequency domain needs to be converted to time-domain for image reconstruction
- Resolve multi-speed issue of electromagnetic (EM) waves using frequency-dependent velocity (phase velocity), unlike traditional radar algorithms that assume all frequency components propagate at the same velocity.
- Resolve the multi-decay issue by compensating energy absorption for each frequency component individually.

The proposed technique solves dispersion and transformation issues associated with time-domain radar imaging. Quantitative analysis and comparison with a conventional radar-based algorithm show that the proposed imaging technique can detect different stages of AD more accurately.

## **2. Background and Proposed algorithm**

This section describes the background and proposed algorithm that uses the amplitude and phase information from the reflected and transmitted EM wave for imaging.

## 2.1. Background

The proposed algorithm is based on continuous EM waves propagating through the brain. Pathological changes, such as the accumulation of beta-amyloid plaques and tau tangles, cause changes in the dielectric properties of the area of interest and its surroundings [5]. This affects how EM waves transmit, reflect, and get absorbed in the tissue and, therefore, causes variations in the amplitude and phase of the reflection and transmission coefficients. Depending on the antenna's polarisation, a uniform EM wave generated can either be a transverse electric (TE) or transverse magnetic (TM) wave. The TE waveguide mode is dependent upon the transverse electric waves, distinguished by the fact that the electric vector  $\vec{E}$  will always be perpendicular to the direction of propagation. To derive the relationship between the dynamic dielectric properties due to pathological changes and the transmission phase of the EM wave in TE mode, different layers, as shown in Fig. 1, are used.

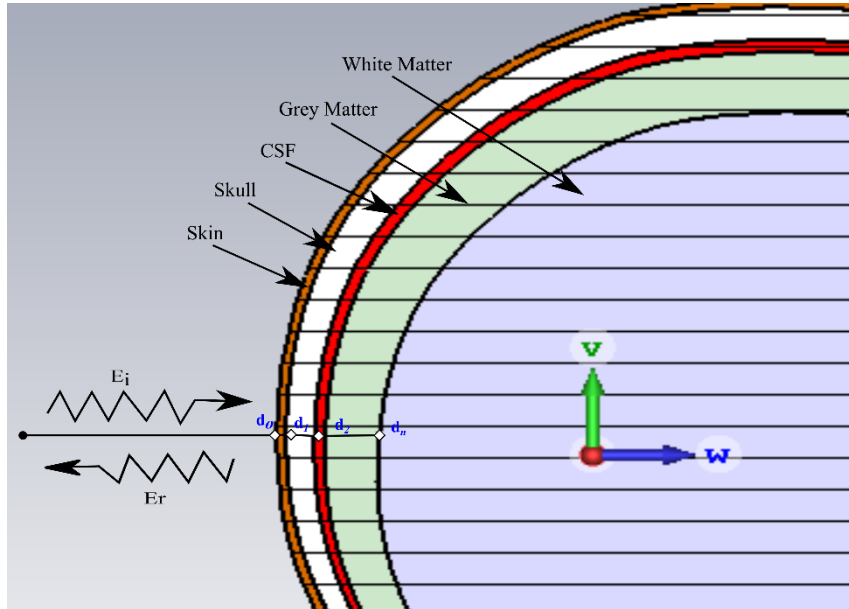


Figure 1: Different layers of a human head model. EM wave propagation is affected due to the difference in the dielectric properties of each layer.

Each layer has dynamic dielectric properties that vary with AD progression, especially small pathological changes in the grey matter and white matter [5]. Furthermore, these tissues are lossy medium due to water-like contents such as fat, blood and CSF. The combinations of the electric and magnetic field in TE mode at the boundary of each layer are given by [17],[18]:

$$E_x(z) = E_{xi}(z) + E_{xr}(z) \quad (1)$$

where  $E_x(z)$  denotes the electric field  $E$  at a reference plane  $x$  and  $z$  is the

direction of propagation,  $i$  and  $r$  represent the incident and reflected signals, respectively. Equation (1) can be rewritten as:

$$= \vec{y} E_{xm} (e^{-jk_x(d_n-d_i)} + R_{x,x+1} e^{jk_x(d_n-d_i)}) \quad (2)$$

where  $k_x = \omega \sqrt{(\epsilon_o \cdot \epsilon_r - j\sigma/\omega) \mu_o}$  is the propagation constant, and  $R$  denotes the reflection coefficients. Similarly, the magnetic field:

$$H_x(z) = H_{xi}(z) + H_{xr}(z) \quad (3)$$

$$= -\vec{x} \frac{1}{n_x} E_{xm} (e^{-jk_x(d_n-d_i)} + R_{x,x+1} e^{jk_x(d_n-d_i)}) \quad (4)$$

where  $n_x = \mu_o/\epsilon_x$  is the wave impedance of the respective layer. Here  $\epsilon_x$  denotes the complex permittivity and is given by

$$\epsilon_x = \epsilon_o \cdot \epsilon_r - j\sigma/\omega \quad (5)$$

where  $\epsilon_o$  is the dielectric constant in a vacuum;  $\epsilon_r$  is the relative permittivity,  $\sigma$  denotes conductivity, and  $\omega$  is the angular frequency and is given by

$$\omega = 2\pi f \quad (6)$$

where  $f$  is the operating frequency. For instance, in layer 3 (CSF), the composition of the electric and magnetic field, where the reference plane  $d = d_2$  is given by

$$E_3(z) = E_{3i}(z) + E_{3r}(z) \quad (7)$$

Here  $z$  is the direction of propagation, and  $i$  and  $r$  denote the incident and reflected field at layer 3, respectively.

$$= \vec{y} E_{3m} (e^{-jk_3(d_n-d_3)} + R_{3,4} e^{jk_3(d_n-d_3)}) \quad (8)$$

$$= \vec{y} T_{2,3} E_{2m} (e^{-jk_3(d_n-d_3)} + R_{3,4} e^{jk_3(d_n-d_3)}) \quad (9)$$

where  $T_{2,3}$  is the transmission coefficient at  $d=d_1$ , and  $R_{3,4}$  is the reflection coefficient at  $d=d_2$ .

Similarly, the magnetic field is given by

$$H_3(z) = H_{3i}(z) + H_{3r}(z) \quad (10)$$

$$= -\vec{x} \frac{1}{n_3} E_{3m} (e^{-jk_3(d_n-d_3)} + R_{3,4} e^{jk_3(d_n-d_3)}) \quad (11)$$

$$= -\vec{x} \frac{1}{n_3} T_{2,3} E_{2m} (e^{-jk_3(d_n-d_3)} + R_{3,4} e^{jk_3(d_n-d_3)}) \quad (12)$$

where  $R_{3,4}$  is the reflection coefficient at  $d=d_2$ , and  $T_{2,3}$  is the transmission coefficient at  $d = d_1$ .

It is worth noting that the transmitted signal  $T_{2,3}$  depends upon  $T_{1,2}$ , which depends

upon the incident signal. The phase of transmission and reflection coefficients are used to estimate the phase change in the respective layer. Assume that  $N$  antennas in total are used. The number of multistatic channels is  $N \cdot M$ . In this  $mn$  channel, assume the phase of signal collected by the  $n$ th receiver is  $\Phi_r$  the phase after compensation  $\Phi_c$  should be

$$\Phi_c = \Phi_r + \Delta\Phi_r \quad (13)$$

where

$$\Delta\Phi_r = (\partial_t + \partial_r)k \quad (14)$$

Here,  $\partial_t$  is the propagation distance from the transmitter to the boundary of each layer,  $\partial_r$  is the distance from the boundary of each layer to the receiver, and  $k$  is the complex wavenumber as a function of frequency.

The value of  $k$  is constant for a lossless medium such as free space, i.e., the known distance from the antenna to the boundary of the head phantom.

In lossy media such as brain tissues, the value of  $k$  shall be

$$k = \alpha - j\beta \quad (15)$$

where

$$\alpha = \omega \sqrt{\frac{\mu\varepsilon}{2}} \left[ \sqrt{1 + \frac{\sigma^2}{\varepsilon^2 \omega^2}} + 1 \right]^{\frac{1}{2}} \quad (16)$$

and

$$\beta = \omega \sqrt{\frac{\mu\varepsilon}{2}} \left[ \sqrt{1 + \frac{\sigma^2}{\varepsilon^2 \omega^2}} - 1 \right]^{\frac{1}{2}} \quad (17)$$

ere  $\omega$ ,  $\mu$ ,  $\sigma$ , and  $\varepsilon$  are the angular frequency, permeability (constant at microwave frequencies), conductivity, and permittivity at a particular frequency.

The real part  $\alpha$  determines the real wavenumber  $k$  used for PS compensation. The imaginary part  $\beta$  causes amplitude decay of wave propagating through a lossy medium, thus compensating both PS and amplitude decay due to absorption in the lossy medium. The complex value of  $k$  solves the multi-speed and multi-decay issue due to dispersion.

In time-domain radar-based algorithms, the distance values are used to calculate the TS, assuming an average propagation velocity for all frequency components. The TS is replaced with PS, similar to [11]. However, the multistatic mode is used to address the dispersion issues. Since PS is compensated for each discrete frequency point separately, and absorption is treated based on frequency-s-dependent velocity; the algorithm solves multi-speed

and multi-decay issues when EM wave propagates through dispersed and lossy media. Dispersion also leads to multi-path issue, which is usually ignored due to the inherently unknown nature of EM wave propagation. In the proposed algorithm, the fastest path using Fermat's principle is used to address the multi-path issue [19].

## 2.2. Proposed algorithm

The proposed algorithm is based on DAS; however, this algorithm uses frequency-domain signals, unlike DAS, which uses reflected or transmitted signals in the time domain. Therefore, the propagation distance values are used to shift the phase of corresponding signals with respect to frequency. Due to the dispersion properties of brain tissue, the incident wave does not propagate along a straight path to the object of interest. In fact, different components of the EM wave can take different paths with different velocities. Moreover, the amplitude decay varies due to variations in dielectric properties. Conventional DAS algorithms cannot accurately detect the time delay between the antenna and object(s) of interest since it assumes that all frequency components of the UWB signals travel at the same speed and path. Therefore, each frequency component must be treated individually for PS between the antenna and a focal point.

The Proposed frequency-based multistatic imaging algorithm contains the following steps:

1. The frequency domain scattered signals obtained using  $N$  antennas placed at equal distances around the head phantom are imported to MATLAB.
2. A common practice to validate the imaging results is to subtract signals received from an empty skull model to remove strong skull reflections. This method improves the accuracy of resulting images; however, it cannot be used in real scenarios. The average subtraction technique is applied to remove outer head layers (skin, skull) reflections to both reflected and transmitted signals separately [13]. The absolute average values for each frequency step were used for subtraction to ensure that the phase values remained intact. The signals are first averaged and then subtracted from signals received at each antenna in the antenna arrays:

$$A_{ij} = \left\{ \begin{array}{l} S_{ii} - \left| \frac{1}{N} \sum_{i=1}^N S_{ii} \right| \\ S_{ij} - \left| \frac{1}{N(N-1)/2} \sum_{\substack{i=1 \\ j \neq i}}^{N(N-1)/2} S_{ij} \right| \end{array} \right\} \quad (18)$$

where  $N$  denotes the number of antennas used for data collection.  $A_{ij}$  is the resulting averaged signals,  $S_{ii}$  denotes the reflected signals, and  $S_{ij}$  denotes the transmitted signal.

3. The relative dielectric constant  $\epsilon$  of the imaging area was estimated for each layer. The effective permittivity of each focal point within the head varies depending on the signal's point of entry and the distance from the boundary of the phantom. The relative dielectric values are computed by analysing the arrival time of signals from the entrance point over the head surface, similar to [19]. The length of the propagation path was calculated using the estimated relative dielectric constant and the radiation mode shown in Fig. 1. According to Fermat's principle, the wave propagates along the fastest propagation path. Therefore, the propagation distance from a transmitting antenna  $t_x$  to a particular position  $r$  in the imaging area and that specific position to the receiving antenna is calculated as

$$\partial_t = \min_r(t_x - r) \quad (19)$$

and

$$\partial_r = \min_r(t_r - r) \quad (20)$$

where  $t_x$  and  $t_r$  are the known antenna positions in Cartesian coordinates, and  $r$  denotes a focal point in the imaging area.  $\partial_t$  and  $\partial_r$  are the propagation distance from the antenna to different layers of the brain and then to receiver antennas, respectively. These values are not based on the thickness of layers and are not known in advance. In fact, the propagation distance from the transmitting antenna to each focal point and then to the receiving antenna is calculated, which is similar to the DAS-based algorithms. The minimum distance is used to address the multi-path issue associated with EM wave propagation in layered and dispersive media. These distance values are used to compensate for the phase values at the corresponding frequency using (14).

4. Estimate the PS using (13) and assuming  $N$  antennas transmitting the signal and received by  $M$  antennas. PS is calculated from each antenna to the focal point using the propagation path. The  $\Delta\Phi_r$  is consistent at each layer and changes with the dielectric properties at the adjacent layer.
5. The delay-and-sum back-projection algorithm is employed for image reconstruction. The phase-compensated signals  $A_{ij}$  obtained in step 4 are summed from all angles based on antenna locations as

$$\text{Image}(r) = \int_{f_{min}}^{f_{max}} \sum_{Ch=1}^{N \times M} A_{i,j} \cdot e^{j\Phi_c(i,j)} \quad (21)$$

where  $Ch$  represents the number of channels between the  $N$  transmitter and  $M$  receivers. Summing these values from all angles (for all antennas) gives power density at a focal point  $r$ . The integration of two or more phase-shifted signals, having a large phase difference, will have a small magnitude when summed. Conversely, the integration of signals (vector addition) having a small difference in phase results in a large magnitude value. Therefore, integrating these values over the minimum to maximum frequency components of the UWB signal represent the energy for a specific position  $r$ . The values are normalised between 0 and 1, showing the lowest and highest color intensity, respectively. These normalised values are then plotted for each point to produce an image with a linear colormap of the 2D cross-sectional area of the head phantom.

### **3. Algorithm Validation**

Experiments were performed on fabricated phantoms to detect the different volumes of plaques and tangles affected tissue in the brain to validate the proposed algorithm. The data obtained from experiments were then used to verify the imaging results.

#### **3.1. Phantoms Used**

Phantoms are often created for imaging human tissues such as the breast and the brain by using materials that mimic the properties of surrounding tissues and the object of interest, such as a malignant tumour or stroke. It provides more consistent results and avoids exposure towards a living human. As a result, phantoms are mainly used for experimental studies and ex-vivo validation of antennas and imaging algorithm results [20]. This study used post-mortem brain tissues with severe AD to measure the dielectric properties. The tissue was taken from the brain's frontal cortex region, which contained a significant number of plaques and tangles, indicating severe AD. The dielectric properties were obtained separately for grey matter and white matter in a frequency range of 0.2 GHz to 3 GHz and compared with those of a healthy brain, as shown in Fig. 2. The four-pole Cole-Cole model was then used to measure the frequency-dependent complex relative permittivity. These measured dielectric values are used to create three phantoms that represent the human brain with different volumes of brain tissue affected by plaques and tangles. The purpose of creating these phantoms is to mimic the dielectric properties of different stages of AD at a specific bandwidth. Fig. 3 shows a fabricated phantom used to validate the proposed algorithm. Experiments were performed on these phantoms using textile-based RF sensors presented in our previous study [1]. The experimental data obtained from these

phantoms are used to reconstruct brain images showing different volumes of AD-affected brain tissues.

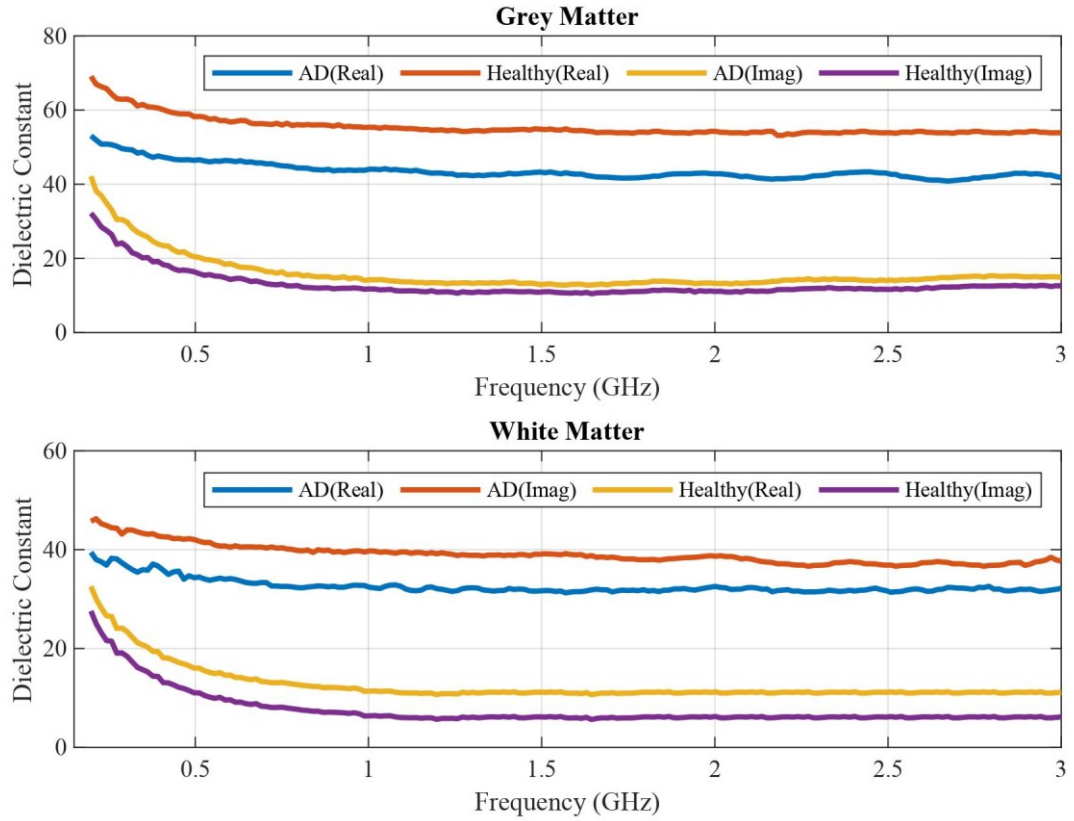


*Figure 2: Measured dielectric constant of the white and grey matter section of AD vs healthy human brain tissue.*

### 3.2. Experiments

A wearable and portable device in a hat-like shape is used for experiments. The sensor's design is based on a rectangular planar monopole antenna structure. The substrate of the antenna is made using a flexible textile, and the conductive part of the antenna is made using a 6 mm thick material. It operates from 1 to 3 GHz and exhibits a radiation pattern of 6 dB front-to-back ratio at central frequency. A 0.1 mm thick conductive textile was used as a dielectric medium between antennas and observers to maintain the integrity of the antennas. A Vector Network Analyzer (VNA) is used to generate and receive the signals. The generated signals are sent to a PC for further processing. Further information on the complete and integrated system consisting of hybrid silicone-textile sensors, switching systems, VNA, and a PC can be found in our previous work [1].

The fabricated phantom mimics the progression of AD-affected tissues in the brain. Each phantom contains three layers, including grey matter, white

matter, and an object of various sizes to represent the AD-affected tissue. Each layer in the phantoms was fabricated separately to create a replica of an adult human brain. Tap water, sugar, and agar powder were used

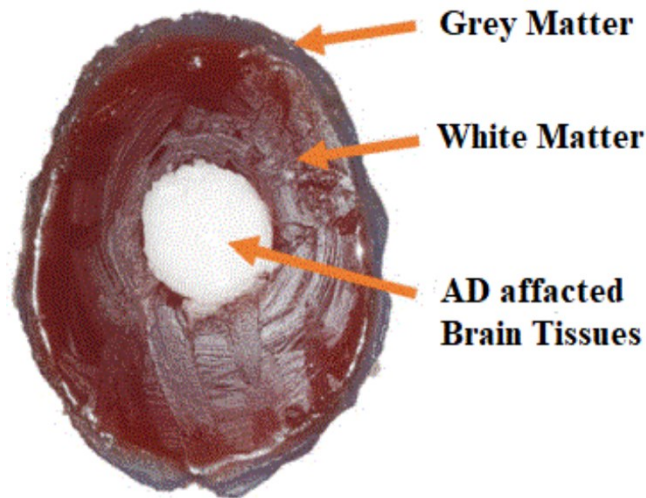


*Figure 3: The cross-sectional view of the fabricated phantom showing the grey matter, white matter, and AD-affected tissue object (white) embedded in the phantom used in experiments.*

to mimic these layers of the brain. Different volumes of AD-affected tissue were embedded in the brain phantoms to emulate the spread of plaques and tangles. The volume of the AD-affected tissue used in this paper is  $22.66 \text{ mm}^3$  for mild,  $113 \text{ mm}^3$  for moderate, and  $226 \text{ mm}^3$  for the severe stage of AD. These various volumes of mock objects are used to investigate if AD changes in the brain could be detected with the proposed algorithm.

To perform the experiments, each phantom with the embedded plaques and tangles objects with varying sizes are placed in the skull model and encircled with the antenna array. Each antenna transmits an EM signal one by one, and the scattered signals are collected by all other antennas. The collected data were imported into MATLAB for further processing and image reconstruction.

The change in both reflected and transmitted signals are used in the proposed algorithm. These signals change due to the different sizes of plaques and tangle objects having different dielectric values than surrounding tissues. The reflected signal change results of one antenna for all cases can be found in Fig. 4.

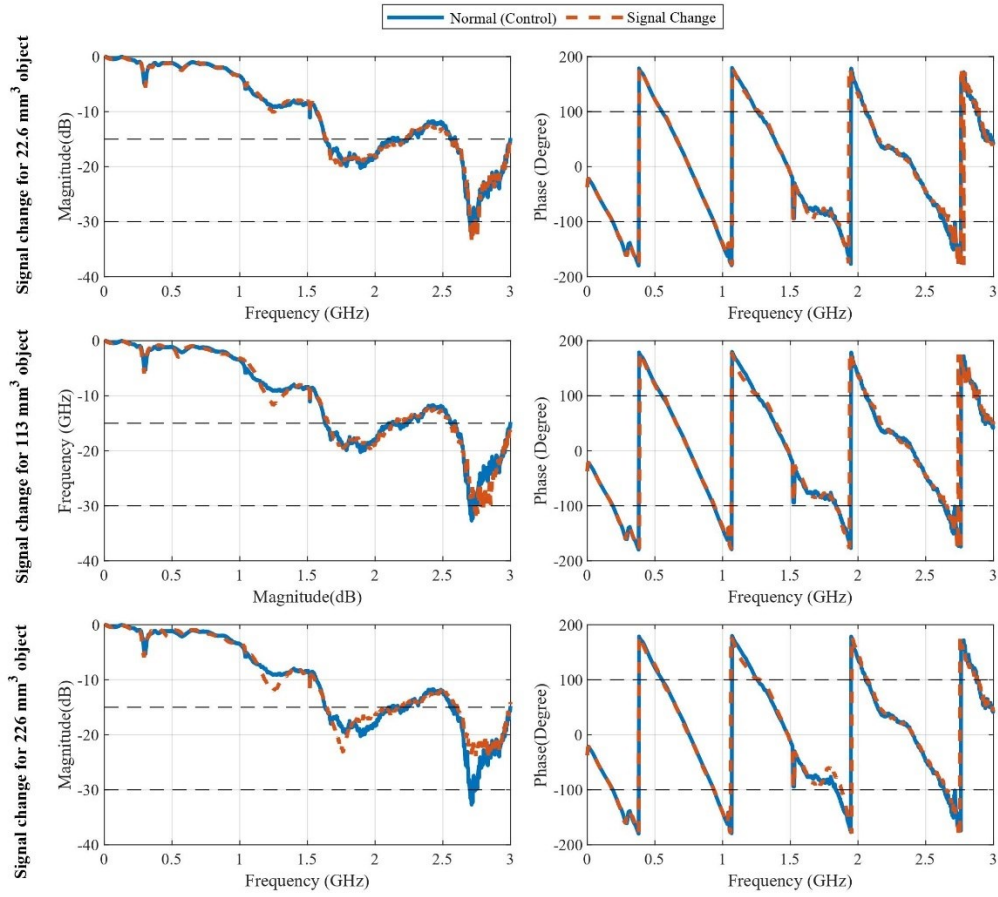


Figure 4: The amplitude and phase of the reflected signal (S11) for the Normal brain

Fig. 4 indicates an almost invisible difference in the phase of reflected signals since all transmitters use the same detection signal; however, there is a 180-degree shift in the signal for each consistent layer. There is a slight difference in the phase around 1.8 GHz due to varying size AD-affected tissue objects used in experiments. Therefore, changes in the phase of both the reflected and transmitted signals are used in the imaging algorithm to realise the boundaries of different layers in the brain. On the other hand, there is more loss in amplitude. This loss in the amplitude of the reflected signal ensures that the antennas are working correctly. The energy loss is due to the plaques and tangle objects with water-like contents that absorb the signal. It can also be observed that there is more loss in the signal on higher frequencies than lower frequencies. The DAS-based algorithm does not consider frequency-dependent attenuation. Instead, all the components of the UWB signals are treated similarly. The strong reflections are used to differentiate tumour or stroke; however, this difference is not big enough to classify AD stages. This is further described in experimental results comparisons in section 5.

The signals were obtained in the multistatic mode, where one antenna transmitted the signal, and reflected and transmitted signals were captured by all other antennas. The experiments were repeated for each antenna to capture both the reflected signals (S11) and transmitted signals (S21). A total number of 201 frequency points were stored for each antenna. Each reflected and transmitted signal has a magnitude (dB) and phase (degree) value at the corresponding frequency. These points were organised as a matrix for each case. The data format is similar for all three stages.

#### **4. Image Reconstruction**

The proposed imaging algorithm is implemented in MATLAB. The resulting data obtained from experiments are used to reconstruct the images that show different volumes of plaque and tangle objects. The amplitude and phase variations in the frequency domain are used to map the pathological changes in the internal layers of brain tissues. The changes in the amplitudes and phase are mapped using steps described in section 2.2 to a two-dimensional plane that shows regions of dielectric contrast.

Fig. 5 shows the resulting images reconstructed for three different volumes of plaques and tangles objects. It can be observed that different layers of the brain are correlated with a different shade in the resulting image; however, the layers are distorted. There is a slight error on the edges of the imaging results. The rationale for these distortions is the smaller number of antennas used. It can also be observed that the outer layer is overlapped due to minimal change and the smaller volume of the skull and skin layer along with antenna couplings. This is typically removed by subtracting skull reflection from an empty skull model; however, the algorithm is not valid in real scenarios [10]. Other techniques are subtracting the average of neighboring antennas to avoid antenna coupling in the monostatic mode of operations [21]. The average subtraction is used separately for reflected and transmitted signals. The absolute average values are used to remove noise and antenna coupling to ensure that phase values are not altered.

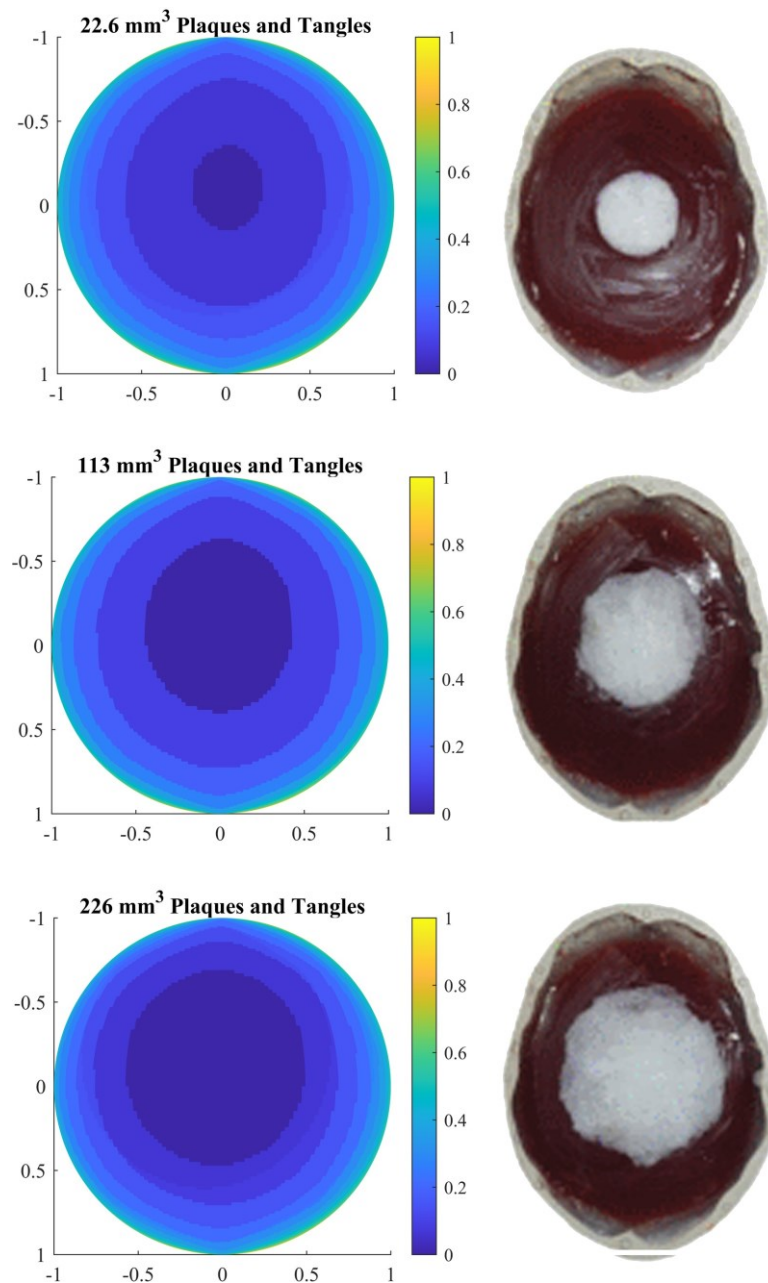


*Figure 5: Resulting images for three AD-affected brain tissue using data from experiments on phantoms (left) and the actual phantoms with different sizes of AD tissue (right). The x-axis represents the left and right and y-axis represents the back and face of the head phantom.*

Despite removing the strong skull reflections (using signals obtained from an empty skull model), the resulting images show changes in the volume of plaques and tangles with reasonable accuracy. The imaging results also demonstrate that the PS-based calculation can adequately mitigate the issues with DAS-based algorithms. The algorithm detects small changes in the internal layers without relying on the accurate TS to align the

reflected/transmitted signals. These results can be improved by using more antennas and highly sophisticated pre-processing techniques for clutter removal. There is a trade-off between the accuracy and efficiency of the algorithm. Increasing the number of antenna and data points and the type of operations, i.e., monostatic or multistatic, will increase the image reconstruction time and accuracy and vice versa. This is further explained in section 5.

To quantify the accuracy of the resulting images, estimation factor and localisation error are used similar to [22]. The estimation factor  $\xi$  estimate the difference between the actual  $v_A$  and detected volume  $v_D$  of brain tissue for different cases as

$$\xi = \Delta v_A / \Delta v_D \quad (22)$$

The localisation error  $\ell$  measures the displacement in the reconstructed images  $V_r$  to the known actual changes  $V_a$  in different layers of tissues in the phantoms for different AD cases. It is calculated using the Euclidean distance from the centre to the boundary of AD-affected tissue as:

$$\ell = \| V_r - V_a \| \quad (23)$$

The results are listed in Table 4.

Table 1: Quantitative analysis of actual and reconstructed images using Estimation factor and sLocalisation error.

	22.6 mm <sup>3</sup> object	113 mm <sup>3</sup> object	226 mm <sup>3</sup> object
$\xi$	0.8	1.1	1
$\ell$	4	5.2	5.3

The value of estimation factor  $\xi$  indicates that the proposed algorithm can accurately detect changes made to the phantoms compared to the reconstructed images. The minimal difference is caused by irregularity in experiments and less number of antennas used. The values are computed based on known values for different cases of AD. Similarly, the localisation error varies from 4 mm for 22.6 mm<sup>3</sup> to a maximum of 5.3 mm for detecting 226 mm<sup>3</sup> plaques and tangles objects. It can be observed that the localisation error is generally higher and can be reduced by using more antennas around the phantoms.

## 5. Discussion and Comparison

Microwave-based medical devices and imaging techniques have been widely

investigated due to their wearable and portable nature. There is a lot of research aiming to detect abnormal tissues, such as breast cancer and brain stroke [23] [24]. Recently it has been discovered that there is a significant difference between the dielectric properties of healthy and AD-affected tissue [5]. These changes can be monitored using EM wave propagation through the human head [25]. This allows the detecting small pathological changes in the brain caused by AD.

Many factors affect the results of any microwave imaging system. The proposed algorithm relies on the correct estimation of phase values. The phase difference between adjacent antenna positions is affected by the antenna's position, spacing between antennas, the permittivity of the propagation medium, and the pulse frequency. As a result, there is no one answer for the required spatial sampling that applies to all brain geometry and tissue composition. When compensating for common artefacts in the frequency domain, i.e., amplitude and phase difference, antenna positions and spacing should be chosen carefully as they might create antenna couplings.

The wavelength of EM waves inside the phantom is relatively short compared to the signal in the same frequency in free space due to a change in velocity. Therefore, it is also of paramount importance to choose suitable antennas. Furthermore, tissue parameters such as permittivity, permeability, and speed are typically dependent on frequency, and higher frequency contents are unsuitable for deeper penetration. These properties also affect the propagation loss, and in complex tissue layers such as the human brain, these losses are even more. Therefore, in layered and dispersive media such as the human head, the observation space (AD-affected brain tissue in this work) becomes opaque. Thus, the traditional radar-based algorithms that ignore multi-speed, multi-path and multi-decay issues cannot explore the inner structure.

The basic principle of the proposed algorithm is based on radar-based imaging algorithms; however, it is different in many ways. The signals in radar-based imaging algorithms are reconstructed into images using various beam-forming techniques based on DAS. These algorithms, such as DMAS and MIST, are improvements to the DAS. However, all these algorithms do not consider the frequency-dependent properties of EM wave propagation. The reflected signals (in monostatic mode) or transmitted signals (in multistatic mode) are first thoroughly delayed assuming that all the frequency components propagate simultaneously. The aligned signals are then summed to reconstruct the image of the object(s) under test. Most of these algorithms operate in the time domain, where the signals obtained in the frequency domain are converted to the time domain using transformation techniques. The proposed algorithm is implemented in the frequency domain and does not rely on an inverse transform that requires the estimation of the correct samplerate.

Furthermore, the DAS-based algorithms use only magnitude information in the time domain (real numbers). In contrast, the proposed algorithm utilises

both the amplitude and phase values (complex numbers) of the scattered signals. The DAS (and its extensions) also ignores the multi-decay issues and assumes all frequency components attenuate at the same level, leading to inaccurate object detection, especially if embedded in dispersive media, such as human head tissues. Therefore, to address these issues, the proposed algorithms treat each frequency component separately for PS compensation and use the frequency-dependent velocity of EM waves to address the multi-decay issue. The propagation distance is calculated for each wave to a focal point in the imaging area. Since attenuation is frequency-dependent, the absorption for each focal point is computed based on propagation distance. In short, the measured scattered field, compensated for frequency-dependent PS and attenuation (due to absorption), from all antennas are summed together and integrated over the frequency range to calculate the value of a focal point.

Fig. 6 shows the reconstructed images using the MIST and DMAS in comparison with the proposed algorithm. It can be observed that the signal for the MIST and DMAS were first converted to the time domain using the Fast Fourier transform (FFT) and subtracted from an empty skull reflection to remove clutter. This technique, though not applicable in real scenarios, is widely used to validate imaging results. The proposed method uses a more realistic method (average subtraction) for clutter removal instead of empty skull reflection. The accuracy and effectiveness of the proposed algorithm can be realised from these images. These algorithms cannot accurately determine the size and shape of the embedded object even after clutter removal. On the other hand, the proposed algorithm detects small pathological changes in the brain due to AD more accurately.

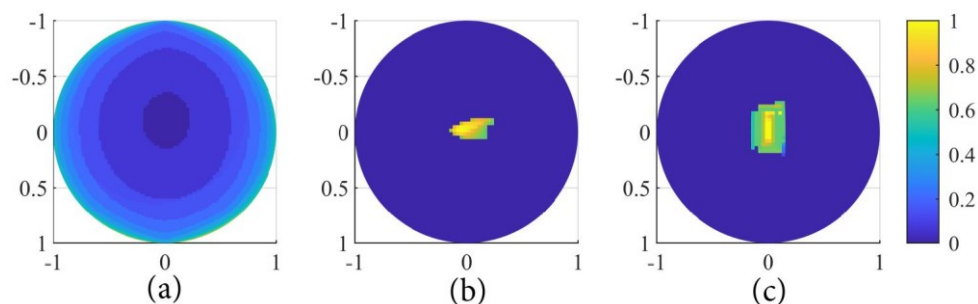


*Figure 6: Resulting images for 22.6 mm<sup>3</sup> Plaques and tangle objects embedded in the phantom (a) With the proposed frequency-based algorithm, with clutter (b) With MIST.*

The DAS-based algorithms square the energy values obtained after summation and rely on the correct alignment of reflected or transmitted signals. However, in many applications, such as biomedical imaging, the objects under test are embedded in a strong, multi-path environment. Therefore, assuming the average speed and the same path and decay for all components of the UWB signal prevents these algorithms from accurately analysing or detecting small changes. It can be

observed that all three algorithms can detect the smallest (22.6 mm<sup>3</sup>) object. However, the shape of the reconstructed object is distorted in DAS and MIST because of ignoring the dispersive behaviour of the Human head tissues.

Another critical factor is efficient image reconstruction, which includes the time from data acquisition to image reconstruction. The computational time of the imaging algorithm plays an important role. The importance depends on the situation. For example, the computation time is of paramount importance in the case of stroke detection as the patient seeks urgent help. Various algorithms are used to improve computational efficiency, such as hardware resources, including graphical processing units, field-programmable gate arrays [26] and software frameworks such as Spark and Hadoop [27]. For applications like AD monitoring, the computation time becomes less important than accuracy.

In terms of computational complexity, the processing time, which includes calculating propagation path, phase and amplitude compensation and summation and integration of multi-frequency signal to reconstruct an image, takes a few seconds. The multistatic nature of the proposed algorithm makes it more complex; however, it overcomes several disadvantages of time-based DAS algorithms that make it worth increasing the computation time. Unlike other DAS-based algorithms, the inverse transform is avoided in the proposed algorithm, and the results are not dependent on choosing an appropriate sample rate. Therefore, it avoids the  $O(N \log N)$  operations required for one signal with  $N$  samples. However, the total computational time is affected by the time needed to calculate the PS values that depend on the number of discrete frequency points in the measured signals. Therefore, the computation complexity with respect to the number of frequency samples is calculated. Simulations data (using six antennas) were used as input to the imaging algorithm, and the execution time for different frequency points was noted. The reason to use simulation data is the unavailability of experimental data, as the experimental data contain only 201 frequency points. Empirical results of the execution time of the proposed algorithm are shown in Fig. 7. The obtained curve shows a linear increase in execution time with the increase in the number of measured frequency points. Using a GPU, C/C++ implementation, or framework such as Hadoop/Spark could reduce the execution time. The average execution time of the proposed algorithm is around 90 seconds, which is approximately similar to time-domain radar-based algorithms [28]. The execution time only contains the image reconstruction time on a personal computer (Core i7-3770 CPU @ 3.40 GHz and 16 GB of RAM).

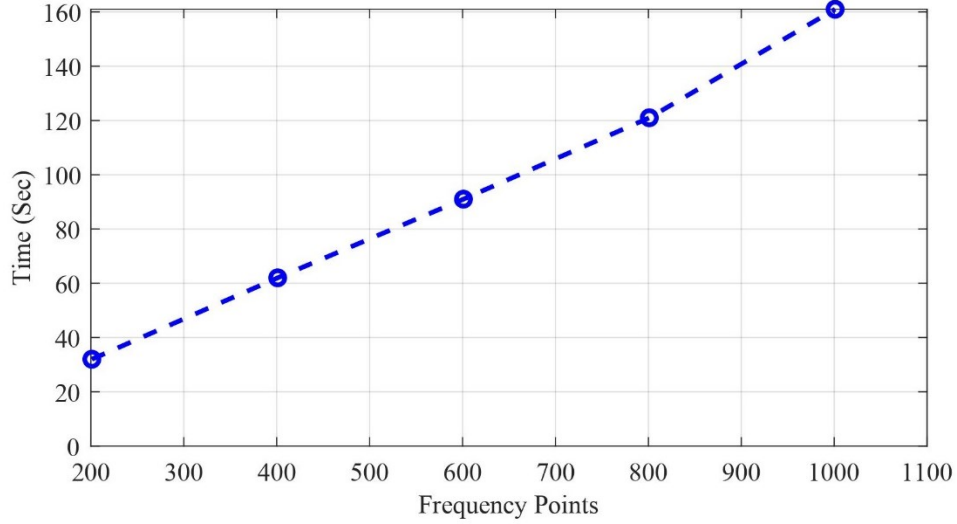


Figure 7: Execution time of the proposed algorithm for different frequency points

Furthermore, the Specific Absorption Rate (SAR) was calculated to investigate the effect of EM waves on the biological tissue, i.e., the human brain. There are safety concerns about the effects of electromagnetic radiation on human tissues. Though RF is not ionising, the transfer and absorption of energy in biological tissue can be potentially harmful if not being cautious. According to the UK government, the maximum limit of SAR is 2 W/kg for 10 g of tissue mass. SAR is a measure of power absorbed per unit mass of human tissue and can be calculated as

$$SAR = \int_{sam} \frac{\sigma(r)|E(r)|^2}{P(r)} d_r \quad (24)$$

where  $\sigma$  denotes electrical conductivity and  $P$  and  $V$  indicate sample density and volume, respectively. The SAR was calculated in CST using (24). The computed value at 1.5 GHz is 0.0115 W/kg for 1 mW and 1.15 W/kg for 100mW. Similarly, at 3 GHz, the calculated SAR values are 0.135 W/kg and 1.355 W/kg for 1 mW and 100 mW, respectively, ensuring that these values are below the specified limit.

## 6. Conclusion and Future Work

A new algorithm is proposed based on the amplitude and phase variations of scattered signals due to changes in the dielectric properties of complex layers of brain tissues. The algorithm compensates both the amplitude and phase of the scattered signals individually and integrates all frequency components for image reconstruction. The algorithm resolves multi-speed, multi-path and multi-decay issues due to dispersion and therefore outperforms the time-shift based approaches. The algorithm was tested to detect pathological changes caused by beta-amyloid plaques and tau tangles in the brain. The data were obtained using six directional antennas from fabricated phantoms based on

complex dielectric values obtained from real post-mortem tissues. The imaging results indicate that the proposed algorithm is robust and detects the changes with sensible accuracy. Comparison with radar-based imaging algorithms that used time-shift of reflected or transmitted signals reveals that the proposed algorithm is more accurate. Furthermore, the algorithm avoids the Fourier transforms, and the reconstructed images do not depend on selecting an appropriate sample rate.

One limitation of the proposed algorithm is that it ignores the multi-path issue due to refraction at the boundary of each layer. Although the least-time method is used to address this kind of multi-path issue, further investigations are required. The imaging results could be improved with more antennas and sophisticated pre-processing techniques for clutter removal. Compared to the actual images, the reconstructed images are not completely accurate. Since the reflection and transmission data is used, there is a question of propagation or depth of the RF signal in the head tissues and how much it penetrates through. Therefore, fabricating a more sensitive (high-resolution) antenna that will capture the volume or depth of the tissues would also improve the accuracy of the resulting images. Future work will be focused on optimising the proposed imaging algorithm and considering more antennas for experiments. Other than average subtraction, pre-processing techniques could also be investigated to remove skull reflections as in traditional radar-based approaches. The evaluation of the quality and accuracy of the resulting images using more sophisticated methods could also be considered in the future. Furthermore, the proposed algorithm will be evaluated as part of portable and wearable microwave imaging systems clinically in future.

## 7. References

- [1] I. Saied, T. Arslan, S. Chandran, C. Smith, T. Spires-Jones, and S. Pal, "Non-invasive RF technique for detecting different stages of Alzheimer's disease and imaging beta-amyloid plaques and tau tangles in the brain," *IEEE Transactions on Medical Imaging*, vol. 39, no. 12, pp. 4060–4070, 2020.
- [2] V. L. Villemagne, V. Doré, S. C. Burnham, C. L. Masters, and C. C. Rowe, "Imaging tau and amyloid- $\beta$  proteinopathies in Alzheimer disease and other conditions," *Nature Reviews Neurology*, vol. 14, no. 4, pp. 225–236, 2018.
- [3] J. C Vickers *et al.*, "Defining the earliest pathological changes of Alzheimer's disease," *Current Alzheimer Research*, vol. 13, no. 3, pp. 281–287, 2016.
- [4] T. Grimmer *et al.*, "Beta amyloid in Alzheimer's disease: increased deposition in brain is reflected in reduced concentration in cerebrospinal fluid," *Biological psychiatry*, vol. 65, no. 11, pp. 927–934, 2009.
- [5] I. Saied, M. Bashri, T. Arslan, C. Smith, and S. Chandran, "Dielectric measurements of brain tissues with Alzheimer's disease pathology in the microwave region," in *2019 IEEE international symposium on medical measurements and applications (MeMeA)*, 2019, pp. 1–6.
- [6] R. Ullah and T. Arslan, "PySpark-Based optimization of microwave image reconstruction algorithm for head imaging big data on high-performance computing and google cloud

- platform,” *Applied Sciences*, vol. 10, no. 10, p. 3382, 2020.
- [7] I. Saied and T. Arslan, “Microwave Imaging Algorithm for Detecting Brain Disorders,” in *2019 29th International Conference Radioelektronika (RADIOELEKTRONIKA)*, Apr. 2019, pp. 1–5. doi: 10.1109/RADIOELEK.2019.8733477.
- [8] L. Xanthos, M. E. Yavuz, R. Himeno, H. Yokota, and F. Costen, “Resolution enhancement of UWB time-reversal microwave imaging in dispersive environments,” *IEEE Transactions on Computational Imaging*, vol. 7, pp. 925–934, 2021.
- [9] M. E. Yanik and M. Torlak, “Near-field MIMO-SAR millimeter-wave imaging with sparsely sampled aperture data,” *IEEE Access*, vol. 7, pp. 31801–31819, 2019.
- [10] R. Ullah, I. Saied, and T. Arslan, “Measurement of whole-brain atrophy progression using microwave signal analysis,” *Biomedical Signal Processing and Control*, vol. 71, p. 103083, 2022.
- [11] W. Shao, T. R. McCollough, and W. J. McCollough, “A phase shift and sum method for UWB radar imaging in dispersive media,” *IEEE Transactions on Microwave Theory and Techniques*, vol. 67, no. 5, pp. 2018–2027, 2019.
- [12] A. Zamani, A. T. Mobashsher, B. J. Mohammed, and A. M. Abbosh, “Microwave imaging using frequency domain method for brain stroke detection,” in *2014 IEEE MTT-S international microwave workshop series on RF and wireless technologies for biomedical and healthcare applications (IMWS-Bio2014)*, 2014, pp. 1–3. doi: 10.1109/IMWS-BIO.2014.7032452.
- [13] A. Zamani, A. M. Abbosh, and A. T. Mobashsher, “Fast frequency-based multistatic microwave imaging algorithm with application to brain injury detection,” *IEEE Transactions on Microwave Theory and Techniques*, vol. 64, no. 2, pp. 653–662, 2016.
- [14] W. Shao, A. Edalati, T. R. McCollough, and W. J. McCollough, “A phase confocal method for near-field microwave imaging,” *IEEE Transactions on Microwave Theory and Techniques*, vol. 65, no. 7, pp. 2508–2515, 2017.
- [15] A. Zamani, S. Ahdi Rezaeieh, K. S. Bialkowski, and A. M. Abbosh, “Boundary Estimation of Imaged Object in Microwave Medical Imaging Using Antenna Resonant Frequency Shift,” *IEEE Transactions on Antennas and Propagation*, vol. 66, no. 2, pp. 927–936, Feb. 2018, doi: 10.1109/TAP.2017.2780898.
- [16] A. Al-Saffar, A. Zamani, A. Stancombe, and A. Abbosh, “Operational Learning-Based Boundary Estimation in Electromagnetic Medical Imaging,” *IEEE Transactions on Antennas and Propagation*, vol. 70, no. 3, pp. 2234–2245, Mar. 2022, doi: 10.1109/TAP.2021.3111516.
- [17] J.-K. Wang, X. Jiang, L. Peng, X.-M. Li, H.-J. An, and B.-J. Wen, “Detection of neural activity of brain functional site based on microwave scattering principle,” *IEEE Access*, vol. 7, pp. 13468–13475, 2019.
- [18] D. Keqian Zhang, *Electromagnetic theory for microwaves and optoelectronic*. Germany: Springer, 2008, pp. 80–83.
- [19] A. T. Mobashsher, A. Mahmoud, and A. Abbosh, “Portable wideband microwave imaging system for intracranial hemorrhage detection using improved back-projection algorithm with model of effective head permittivity,” *Scientific reports*, vol. 6, no. 1, pp. 1–16, 2016.
- [20] R. Ullah and T. Arslan, “Detecting pathological changes in the brain due to alzheimer disease using numerical microwave signal analysis,” in *2020 IEEE international RF and microwave conference (RFM)*, 2020, pp. 1–4. doi: 10.1109/RFM50841.2020.9344758.
- [21] A. Zamani and A. Abbosh, “Hybrid clutter rejection technique for improved microwave head imaging,” *IEEE Transactions on Antennas and Propagation*, vol. 63, no.

- 11, pp. 4921–4931, 2015, doi: 10.1109/TAP.2015.2479238.
- [22] A. Brankovic *et al.*, “Unsupervised algorithm for brain anomalies localization in electromagnetic imaging,” *IEEE Transactions on Computational Imaging*, vol. 6, pp. 1595–1606, 2020.
- [23] A. E. Stancombe, K. S. Bialkowski, and A. M. Abbosh, “Portable microwave head imaging system using software-defined radio and switching network,” *IEEE Journal of Electromagnetics, RF and Microwaves in Medicine and Biology*, vol. 3, no. 4, pp. 284–291, 2019, doi: 10.1109/JERM.2019.2901360.
- [24] D. O’Loughlin, M. O’Halloran, B. M. Moloney, M. Glavin, E. Jones, and M. A. Elahi, “Microwave breast imaging: Clinical advances and remaining challenges,” *IEEE Transactions on Biomedical Engineering*, vol. 65, no. 11, pp. 2580–2590, 2018, doi: 10.1109/TBME.2018.2809541.
- [25] J. M. Elloian, G. M. Noetscher, S. N. Makarov, and A. Pascual-Leone, “Continuous wave simulations on the propagation of electromagnetic fields through the human head,” *IEEE Transactions on Biomedical Engineering*, vol. 61, no. 6, pp. 1676–1683, 2014.
- [26] M. A. Mansoori, P. Lu, and M. R. Casu, “FPGA acceleration of 3D FDTD for multi-antennas microwave imaging using HLS,” *IEEE Access*, 2021.
- [27] R. Ullah and T. Arslan, “Parallel delay multiply and sum algorithm for microwave medical imaging using Spark big data framework,” *Algorithms*, vol. 14, no. 5, p. 157, 2021.
- [28] S. S. KaramFard and B. M. Asl, “Fast delay-multiply-and-sum beamformer: Application to confocal microwave imaging,” *IEEE Antennas and Wireless Propagation Letters*, vol. 19, no. 1, pp. 14–18, 2019.